ON WAVE BREAKING IN TUNED LIQUID DAMPERS

Oda T. F.[1,*], Hamed M.S.[1], and Saud Ghani[2]

*Author of correspondence
[1]Thermal Processing Laboratory, Department of Mechanical Engineering,
McMaster University, Hamilton, Ontario, Canada
E-Mail: tareko@mcmaster.ca

[2]Department of Mechanical and Industrial Engineering, Qatar University, Doha, Qatar

ABSTRACT

Tuned Liquid Dampers (TLDs) are passive damping devices used to damp vibration due to wind in tall buildings and due to sea waves in offshore platforms. This paper presents numerical results of wave breaking in TLDs obtained using a numerical model developed in-house. The model solves the full form of Navier-Stokes equations for viscous liquid sloshing and handles the moving free surface by using the volume of fluid method (VOF). Some of the previous numerical models invoke a two-phase flow model in conjunction with the VOF method to simulate the wave transformation and wave breaking in shallow water. However, these two-phase flow models give no account to the effect of body force on the free surface. The current model uses the continuum surface force model (CSF) which models the discontinuity accompanied with wave breaking as a continuous transition where fluid properties such as density vary smoothly from one fluid to another. Numerous experimental studies reveal that the impulse pressure exerted on the tank walls varies in a similar nature as that of the applied excitation. Accordingly, the current numerical model suggests new formulae for the pressure at the left and right TLD walls. The present numerical results are in good agreement with experimental data. The current model is able to accurately detect surface wave breaking at various excitation frequencies.

INTRODUCTION

The use of tune liquid dampers outweighs the use of other passive damping devices from the reliability ,operating and maintenance costs [1,2] and ,of course ,the ability to damp both light scale vibration due to wind [3,4] and large excitation due to sea waves in offshore platforms. TLDs are also used in marine vessels stabilization against rocking and rolling motions [5]. However in due to the use of TLD the optimum damping without additional damping devices will be less than the optimal values. The TLD damping performance has been improved by using rough elements [6], surface contaminants [7] and nets or screens [2, 8, 9]. The most recent application of TLDs in Canada is in the One King West building in Toronto. The 51 storey structure is the most slender structure in the world with an aspect ratio of 11:1[7]. The first attempt towards an accurate prediction of the sloshing-induced dynamic pressures over the internal girders and walls of fuel tanks is due to [10]. Abramson has applied linear theories, based on the potential formulation of the velocity

field, to the analysis of the liquid motion in cylindrical and spherical tanks and in ring and circular sector compartmented tanks [10] as a direct aerospace application. Without any doubt the analysis of [10, 11] postulate the corner stone of many successive numerical and experimental researches of TLDs.

NOMENCLATURE

A	[m]	Amplitude of external dynamic excitation
C*	[-]	Courant time Multiplier
F	[-]	Liquid volume fraction
F_{TLD}	[N]	Total sloshing force on TLD walls
$\vec{F}_{sv}$	[N/m^3]	The Volume force
$\vec{F}_{sa}$	[N/m^2]	The surface force upon an interfacial area
$\vec{F}_b^{\,n}$	[N/m^3]	The body force at the pervious time step
f	[Hz]	Excitation frequency on TLD
g_x	[m/s^2]	Horizontal acceleration
g_y	[m/s^2]	Gravitational acceleration
h	[m]	Height of the initial flat free surface
h*	[m]	The transition Region thickness
H	[m]	The TLD tank Height
L	[m]	The TLD tank length
m_w	[Kg]	The liquid mass inside TLD
p	[N/m^2]	pressure
t	[Sec.]	time
u	[m/s]	The fluid flow velocity component in x-direction
v	[m/s]	The fluid flow velocity component in y-direction
x, y	[m]	Cartesian coordinates
$\vec{V}$	[m/s]	The generalised velocity vector
W	[m]	The TLD tank width
Greek symbols		
η	[m]	Free surface elevation over the nominal fluid height
ρ	[kg/m^3]	Fluid density
μ	[N.s/m^2]	Fluid dynamic viscosity
τ	[N/m^2]	Fluid flow stress
σ	[N/m]	Surface tension
ω	[rad. /s]	Excitation angular frequency

LITERATURE REVIEW

Numerous numerical models have been developed to investigate the sloshing behavior of the liquid inside the TLD. In the early studies [10,12,13] equivalent mechanical models were suggested for both the structure as well as the liquid storage tanks. On the other hand a different way of handling the liquid sloshing numerically was invoked based on the potential flow theory [14] as well as the shallow water wave theory [15]. In fact the potential flow theory has no account for the effect of fluid properties on the sloshing liquid motion. It also can not be used to investigate the fluid flow behavior around obstacles as the created vortices could not be modeled via the potential theory. The shallow water wave theory based on the small wave amplitude compared with the mean depth of the liquid layer was used in many research studies of the TLD [15]. Unfortunately the shallow water wave theory failed to model the flow field around the obstacles in the TLD. Many of numerical techniques use a linear form of the NSE ,which gained by neglecting the convective acceleration terms used in the handling of the sloshing fluid flow motion in case of the external excitation with small amplitudes or with excitation with a frequency away from the natural frequency of the TLD[16]. The linear theory is inadequate in the case of high excitation amplitude as the convective acceleration terms have pronounced effect on the sloshing motion [17]. The numerical methods [11, 18, 19, and 20 involve the solution of Navier–Stokes equations (NSE) for viscous liquid sloshing instead of the shallow water wave theory models provides more accurate results.

THE CURRENT NUMERICAL MODEL

The current numerical model involves prediction of wave breaking. Wave breaking has been studied using the shallow water wave theory employing a non-depressive, fully non-linear wave system [21, 22, 23, and 24]. Although the shallow water theory simulates wave breaking, however, numerical instabilities were noticed inherent in

the rapid change of the breaking wave front [25]. The shallow water theory failed to predict wave breaking due to the treatment of wave breaking as a discontinuity of the free surface in contrast to the physical behavior of the wave breaking, which postulates a rapid transition involving turbulence [25]. In addition, the pressure field is not exactly hydrostatic, especially near the breaking wave front [25]. The current numerical model solves the Navier–Stokes equations (NSE) for viscous liquid sloshing and handles the moving free surface by using the volume of fluid method (VOF) [26, 27, 28]. In contrast to other numerical models [16 and 17] that neglect the convection-acceleration terms, the current numerical model accurately handles the convection acceleration terms. It is noteworthy that the current numerical method handles the jump in the pressure at the interface. The current model carefully evaluates the pressure at the free surface as the pressure is greatly affected by the surface tension and the fluid flow stress gradients [29]. D. Liu and P. Lin [32] introduced for the concept of virtual body force (VBF).The concept of VBF was modified and used in the current numerical technique. The experimental study [31] reveals that the pressure exerted on the walls varies in a similar nature as that of the applied excitation. According to [31], the direct comparison between surface waves and the deep inner waves reflect that the pressures at the walls show a considerable fluctuation near the free surface of the liquid compared to the deeper surfaces in the tank. Moreover the study also shows that although the deep waves were blunt and less steep from the surface waves, but the value of pressure on the fluid element at the location of deep waves will be higher. Accordingly, the current numerical model will assign the pressure at the left and right wall boundaries according to the formulae:

$$p = \alpha p * e^{\left(\frac{-y}{h}\right)} * \sin(\omega t) \quad (1)$$

The factor αp was the parameter defined as the pressure maximum amplitude during the TLD excitation period. This factor, αp, will be affected by the external excitation nature.

THE GOVERNING EQUATIONS AND BOUNDARY CONDITIONS

The model problem is shown in Figure 1. The governing equations of the incompressible , Newtonian ,laminar flow in the Cartesian coordinate system are as follows:-.

The Continuity Equation

$$\frac{\partial u}{\partial x} + \frac{\partial v}{\partial y} = 0 \quad (2)$$

The Momentum Equation In X- Direction

$$\frac{\partial u}{\partial t} + u\frac{\partial u}{\partial x} + v\frac{\partial u}{\partial y} = -\frac{1}{\rho}\frac{\partial p}{\partial x} + g_x + \frac{1}{\rho}\frac{\partial \tau_{xx}}{\partial x} + \frac{1}{\rho}\frac{\partial \tau_{xy}}{\partial x} \quad (3)$$

The Momentum Equation In Y- Direction

$$\frac{\partial v}{\partial t} + u\frac{\partial v}{\partial x} + v\frac{\partial v}{\partial y} = -\frac{1}{\rho}\frac{\partial p}{\partial y} + g_y + \frac{1}{\rho}\frac{\partial \tau_{yy}}{\partial y} + \frac{1}{\rho}\frac{\partial \tau_{xy}}{\partial y} \quad (4)$$

The Free Surface Time Evolution Equation

The time evolution equation of the liquid free surface represented as :

$$\frac{\partial F}{\partial t} + u\frac{\partial F}{\partial x} + v\frac{\partial F}{\partial y} = 0 \quad (5\text{-a})$$

After the velocity and pressure fields are calculated using an assumed liquid volume fraction, F, the liquid volume fraction, F, is updated. The new F-field is calculated by solving equation (5-a), [28]. Combining this equation with the continuity equation gives the conservative form of the F – field, as:

$$\frac{\partial F}{\partial t} + \frac{\partial (F u)}{\partial x} + \frac{\partial (F v)}{\partial y} = 0 \quad (5\text{-b})$$

THE BOUNDARY CONDITIONS

The no-slip and no-penetration boundary conditions are employed at the tanks walls: left hand side wall, the bottom and the Right wall, figure(1).

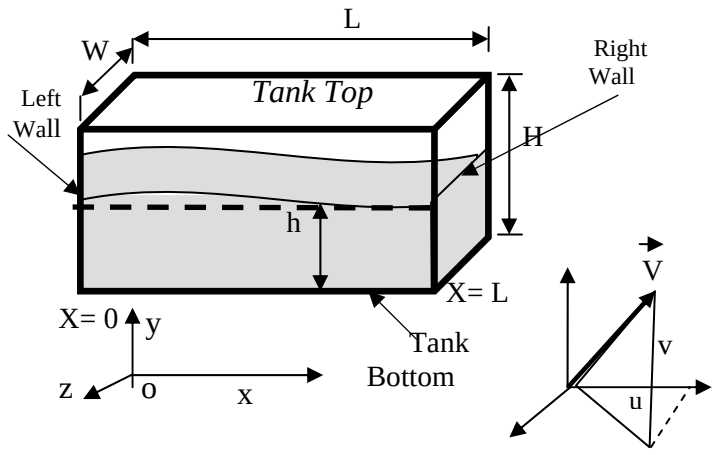

Figure 1 The TLD Basic Dimensions, The Cartesian Coordinate System and The Fluid Flow Velocities

The pressure at the fluid cells in the vicinity of the ghost cells at the bottom wall, have a pressure which equals to the hydrostatic pressure of the fluid and according to the nominal fluid height.

The pressure at the left and right TLD walls as stated earlier:

$$p = \alpha p * e^{\left(\frac{-y}{h}\right)} * \sin(\omega t) \qquad (1)$$

According to the CSF model used in the current numerical model at the interface region between the water surface (fluid 1) and air adjacent (fluid 2), there were a transition region with finite depth within which the fluid properties as density vary smoothly from one fluid to another within the transition region [29].The two fluids are distinguished by some characteristic function, $c(\vec{x})$, which was characterized by:

$$\begin{aligned} c(\vec{x}) &= c_1 \quad , for\ \ fluid(1) \\ &= c_2 \ , for\ \ fluid(2) \\ &= \langle c \rangle = (c_1 + c_2), at\ the\ \text{int}erface \end{aligned} \qquad (6)$$

The fluid density, for instance, of any point within the transition region is evaluated as, $\rho(\vec{x}) = \langle \rho \rangle$. Then the CSF model consider replacement of the discontinuous characteristic function $c(\vec{x})$ by a smoothed variation function, $\tilde{c}(\vec{x})$, of the fluid properties from c_1 to c_2. This variation will be demonstrated over a distance $o(h^*)$, where (h^*) is the transition layer thickness and comparable to the resolution afforded by the calculation mesh size. Accordingly, we replace the boundary values at the interface by a continuous model where the values of (c) at grid points was specified and interpolation process takes place between grid points. The exact surface stress boundary condition at the free surface can be written in tensor form [29],

$$(\sigma\kappa - p_s)\hat{n}_i = (\delta_{ik} - \hat{n}_i \hat{n}_k)\frac{\partial \sigma}{\partial x_k} - \tau_{ik}\hat{n}_k \qquad (7)$$

Where σ is the fluid surface tension, $\hat{n}_i$ is the unit force normal to the surface (into fluid 2), and $\kappa(\vec{x})$ is the local free surface curvature, taken positive if the center of curvature points towards (fluid 2), Figure(2). The projection of the surface stress in tensor form, equation (7) along the unit normal $\hat{n}$ and the unit tangent $\hat{t}$ results in an equivalent set of scalar boundary conditions[29], as:

The normal stress boundary condition given by:

$$p_s - \sigma\kappa = 2\mu n_k \frac{\partial u_k}{\partial n} \qquad (8)$$

And the tangential boundary condition given by:

$$\mu\left(t_i \frac{\partial u_i}{\partial n} + n_k \frac{\partial u_k}{\partial s}\right) = \frac{\partial \sigma}{\partial s} \qquad (9)$$

Where, $\frac{\partial}{\partial s} = \hat{t}.\nabla$ is the surface derivative and $\frac{\partial}{\partial n} = \hat{n}.\nabla$ is the normal derivative.

Moreover the viscous stress on the R.H.S of equation (9) will be neglected as the dominant part to assess the surface tension induces the pressure jump across the fluid interface. The surface tension coefficient σ was assumed constant and accordingly equation (9) will be modified as:

$$p_s = \sigma\kappa \qquad (10)$$

Instead of the direct evaluation of the surface pressure using the Laplace's equation(10), the current model use the CSF model to reformulate the surface tension by using the volume force $\vec{F}_{sv}$ and by using delta function introduced ,[29], as:

$$\lim_{h\to 0} \int_{\Delta V} \vec{F}_{sv}(\vec{x})\, d^3x = \int_{\Delta S} \vec{F}_{sa}(\vec{x}_S)\, d\,S \qquad (11)$$

Where $\vec{x}_S$ is a point on the interfacial area ΔS.

Moreover the surface force $\vec{F}_{sa}(\vec{x}_S)$ was expressed as:

$$\vec{F}_{sa}(\vec{x}_S) = F_S^{(n)}\hat{n} + F_S^{(t)}\hat{t} \qquad (12)$$

Where $F_S^{(n)}$ and $F_S^{(t)}$ are the surface force components along the unit normal ($\hat{n}$) and the unit tangent ($\hat{t}$) respectively, figure (2). In the current numerical work the viscous stresses at the free surface were neglected and the surface tension coefficient σ was assumed to be constant, therefore the surface force around on the interfacial area, $\vec{F}_{sa}$ was equal to the surface force along the unit normal ($\hat{n}$), $\vec{F}_S^{(n)}$. Hence:

$$\vec{F}_{sa}(\vec{x}_S) = \vec{F}_s^{(n)}(\vec{x}_S) = \sigma\,\kappa(\vec{x}_S)\,\hat{n}(\vec{x}_S) \qquad (13)$$

The surface tension force per unit interfacial area, $\vec{F}_s^{(n)}(\vec{x}_S)$, will be added to the body force in the momentum equation:

$$\frac{\partial \vec{V}}{\partial t} + \nabla.\left(\vec{V}\vec{V}\right) = -\frac{1}{\rho}\nabla p + \frac{1}{\rho}\nabla.\tau + \vec{g} + \frac{1}{\rho}\vec{F}_b \quad (14)$$

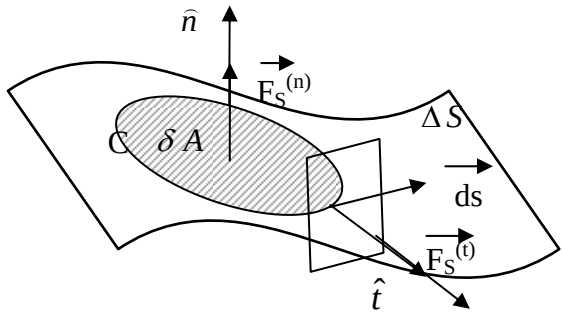

Figure 2 the normal and tangential surface force components at the free surface.

THE NUMERICAL IMPLEMENTATION

Two Step Projection Method

The time discretization form of the momentum equation for incompressible fluid flow will be:

$$\frac{\vec{V}^{n+1} - \vec{V}^{n}}{\delta t} = -\nabla.\left(\vec{V}\vec{V}\right)^{n} - \frac{1}{\rho^{n}}\nabla p^{n+1} + \frac{1}{\rho^{n}}\nabla.\tau^{n} + \vec{g}^{n} + \frac{1}{\rho^{n}}\vec{F}_b^{n} \quad (15)$$

As the pressure gradient was the key to solve the discretized momentum equation, the pressure term was the implicit term in equation (15), while the other terms as advection, body force, and viscous stresses will be evaluated from the previous time step, denoted by the superscript (n).

It follows that two step projection method follow to divide the momentum equation (15) into:

$$\frac{\tilde{\vec{V}} - \vec{V}^{n}}{\delta t} = -\nabla.\left(\vec{V}\vec{V}\right)^{n} + \frac{1}{\rho^{n}}\nabla.\tau^{n} + \vec{g}^{n} + \frac{1}{\rho^{n}}\vec{F}_b^{n} \quad (16)$$

And

$$\frac{\vec{V}^{n+1} - \tilde{\vec{V}}}{\delta t} = -\frac{1}{\rho^{n}}\nabla p^{n+1} \quad (17)$$

The legacy of velocity field $\tilde{\vec{V}}$ at the previous time step, according to the balance between the gravitational force, advection term, and the body forces, equation (16), was evaluated. That velocity field will be corrected by the pressure gradient term at the new time step to extract the new velocity field vector at the new time step, $\{\vec{V}^{n+1}\}$, equation (17). The continuity equation applied for the new time step denoted by the superscript (n+1) will be:

$$\nabla.\vec{V}^{n+1} = 0 \quad (18)$$

Using equation (17) and combined it with equation (18) we extract well known Poisson's equation, for evaluation of pressure gradient, as:

$$\nabla.\left(\frac{1}{\rho^{n}}\nabla p^{n+1}\right) = \frac{\nabla.\tilde{\vec{V}}}{\delta t} \quad (19)$$

One of the important features of the PPE given by (19) is that the pressure gradient adapted by other forces affect the fluid element as the gravitational, body forces, the inertia forces, and the viscous stresses via the acceleration term $\frac{\nabla.\tilde{\vec{V}}}{\delta t}$ will be the corner stone to evaluate the new velocity field at the new time step (n+1), $\vec{V}^{n+1}$.

The Formulation of Wave Breaking

The kinematic boundary of the free surface was given [34], on the assumption of equality of the vertical component of velocity across the interface between water surface and the adjacent air, as well as there were no air cushions in the water side at the interface, and then the kinematic boundary will be:

$$v_{liquid} = v_{air} = \frac{d\eta}{dt} = \frac{\partial \eta}{\partial t} + u\frac{d\eta}{dx} + v\frac{d\eta}{dy} \quad (20)$$

Where the hydrodynamic pressure of the excited liquid free surface was given by the use of Bernoulli's equation, assuming the potential flow theory [34,35]:

$$\frac{p(x,y,t)}{\rho_f} = -\left\{\frac{\partial \phi}{\partial t} + \frac{1}{2}\left|\nabla \phi\right|^2 + g\eta\right\} \quad (21)$$

The former equation based on the potential flow theory and $\phi(x,y,t)$ is the potential function. The current numerical model will replace equation (21) by another formula which gives accountant of the viscous stresses and body forces.

The surface elevation over the nominal fluid height, $\{\eta\}$, was extracted using the potential theory,[41] as:

$$\eta = \frac{1}{g}\left.\frac{\partial \phi}{\partial t}\right\}_{y=h} \quad (22)$$

It could be easily explain that the pressure gradient w.r.t. y-direction at certain x- direction will be equal to the gradient of potential function with y-direction as follows:

$$-\left.\left(\frac{h}{\rho^{n} g}\frac{\partial^2 p^{n+1}}{\partial y^2}\right)\right\}_{y=h} = \left.\frac{\partial \eta}{\partial y}\right\}_{y=h} \quad (23)$$

Equation (23) will be used to detect the location of wave breaking and digitize numerically the onset of formation of wave crest and consequently will be useful in study the effect of wave breaking on the sloshing motion inside TLD tanks.

It is worth noting that the current numerical work replace the use of Bernoulli's equation to assess the dynamic pressure of the excited free surface , where the pressure value was extracted from the potential flow theory , which neglect the fluid viscous forces. Instead the pressure gradient appear in equation (23) which was extracted from direct solution of

Poison's equation (19) and carries , of course, all the legacy of viscous and body forces from the evaluation of $\nabla.\tilde{\tilde{V}}$ directly from equation (16):

$$\frac{\tilde{\tilde{V}}-\vec{V}^n}{\delta t}=-\nabla.\left(\vec{V}\vec{V}\right)^n+\frac{1}{\rho^n}\nabla.\tau^n+\vec{g}^n+\frac{1}{\rho^n}\vec{F}_b^n \quad (16)$$

The streamlines that localize the free surface has a stream function which was a direct function of (x, y, t) as $\psi(x,y,t)$. The wave breaking surface was recognized by folding the wave on itself. The wave breaking is presented in three different events [36]: (I) wave breaking with alternate breaking, (II) wave breaking with long-time randomise asymmetric behaviour, and (III) wave breaking with local splashing jets. All the events accompanied with wave breaking contain the folding wave on itself as a consequence of wave breaking. Therefore there was a point on the surface wave where the streamline of the free surface fold on itself, this point called the "reflection point". For the reflection point the second order differential of the stream function w.r.t. the vertical y-direction will vanish as:

$$\frac{\partial^2\psi}{\partial y^2}=0 \quad ,\frac{\partial\psi}{\partial y}=\frac{\partial\phi}{\partial x},then \quad \frac{\partial}{\partial x}\left(\frac{\partial\phi}{\partial y}\right)=0,hence \quad \frac{\partial\phi}{\partial y}=cons\tan t \quad (24)$$

And hence the second order differentiation of pressure will vanish at the location of reflection point:

$$\left(\frac{\partial^2 p^{n+1}}{\partial y^2}\right)_{y_{at\ the\ reflection\ point}}=0 \quad (25)$$

Equation (25) postulates the criterion of detection of the onset of wave breaking. The detection of wave breaking burden on the pressure gradient to be constant with respect to (y-direction). Consequently the pressure gradient which carries the legacy of the other stresses affects the flow field, as the viscous stresses and the body forces will be a sensitive criterion for the correct detection of the location of the wave breaking.

The Numerical Computation Time Step and The Stability Criterion

The momentum transport equation (15) and the free surface time evolution equation (5) according to the VOF method were explicit equations in time. Hence the calculation time step must be criticized by the Courant time limit. The Courant time step limit in x-direction and y direction will be δt_{cx} , δt_{cy} respectively. The Courant time step limit δt_C should be taken as the minimum of δt_{cx} , δt_{cy} , consequently the computation time step should be evaluated as:

$$\delta t \le \left\{\delta t_C=\min\left(\delta t_{cx},\delta t_{cy}\right)\right\} \quad and \quad \delta t_{cx}=C^*\left\{\frac{\delta x}{|u|}\right\}_{\min.},\delta t_{cy}=C^*\left\{\frac{\delta y}{|v|}\right\}_{\min.} \quad (26)$$

The value of the Courant multiplier (C^*) appear in equation (26) could be taken as 1.0 in theoretical basis, but in practical applications, where the flow field was highly non-linear , the multiplier (C^*) should be taken a value which was in the vicinity of $C^* \le 0.5$. On the current numerical work we select a value of {C^* = 0.3} to ensure stability [1, 20]. Another important stability criterion was selected in due to the diffusion process, so as to avoid the negative diffusion and the computation time step must also satisfied this condition [20]:

$$\delta t \le \min\left(\frac{\rho\,\Delta x^2}{6\mu},\frac{\rho\,\Delta y^2}{6\mu}\right) \quad (27)$$

The current numerical time step was chosen to be $\delta t = 6.62*10^{-4}\ Sec.$

The computer program flow chart will be fully illustrated in figure (3).

The details of the current numerical model was fully illustrated in [37].

MODEL VALIDATION

The validation of the numerical model was invoked by the direct comparison between the numerical evaluation of free surface elevation and the experimental findings [8]. A prototype of a structure building of 1:10 scale was equipped with TLD tank constructed from 19mm thick acrylic with length of 966mm, width of 360mm, and the nominal water height inside was 119mm [8]. The excitation force was applied on the combined system of structure and TLD using a driving spring attached to a hydraulic actuator, the combined system of structure and TLD was tested by applying a sinusoidal excitation. The free surface elevation during the excitation was measured by a wave probe. The other performance parameters as structural acceleration and structural displacement were also measured[8].The excitation imposed was sinusoidal according to the horizontal displacement according to $x = A\sin(\omega t+\varphi)$, where (A) is the excitation amplitude, (A = 25.9mm). The excitation frequency { f }, $\omega = 2\pi f$, $f = 0.594\,Hz$, and the phase shift angle, $\varphi = 4^0$. The wave probe was mounted to detect the excited free surface elevation at a distance { $x = 0.0483\,mm$ } measured from the left hand side TLD tank wall. The direct comparison between the current numerical time history of the wave surface elevation for 30 seconds time span and the experimental findings, [8] exhibit a good agreement which validates the use of the computer program to detect the enhanced free surface elevation under the external excitation, figure (4).

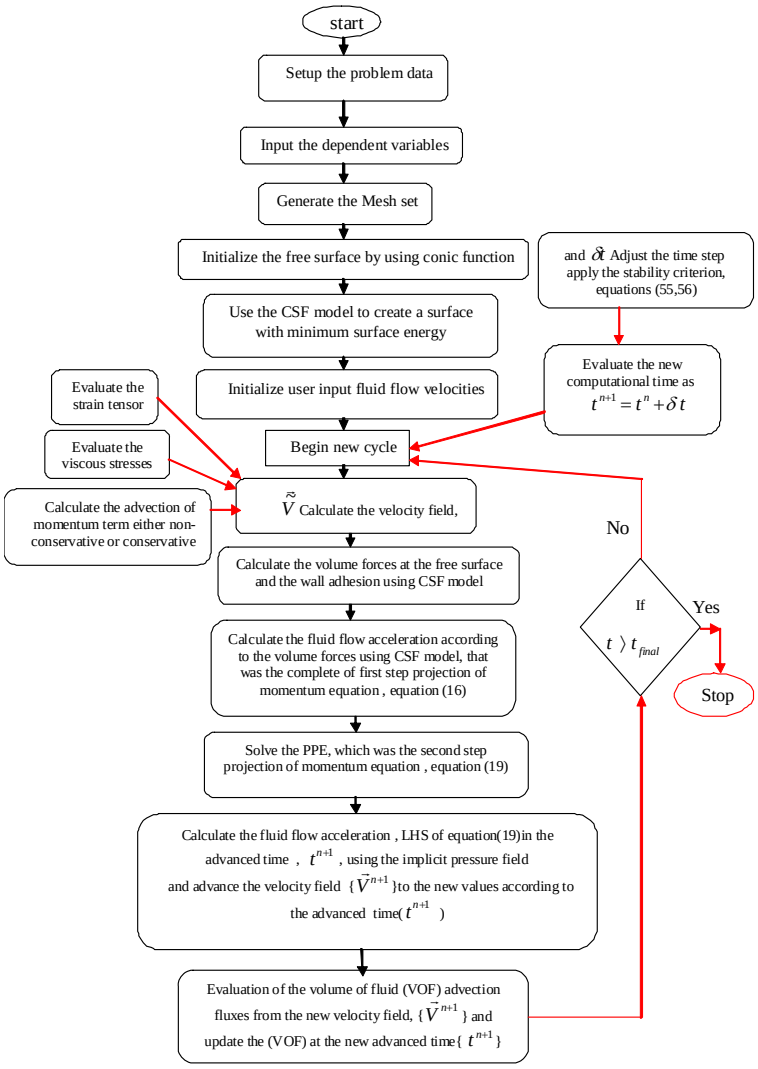

Figure 3 Flow chart of the computer Code

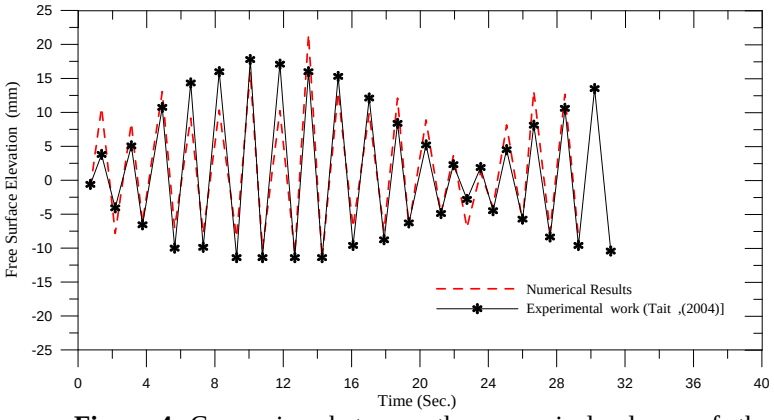

Figure 4 Comparison between the numerical values of the free surface elevation of liquid inside TLD and the experimental findings [7] for excitation with sinusoidal wave of amplitude ,A=0.259 cm and with a frequency of 0.59 Hz., phase shift angle = 4^0.

THE NUMERICAL RESULTS AND DISCUSSION

The Time History Of The Impulse Pressure And The Total Sloshing Force And The Non-Linear Behaviour Of Sloshing Motion

The sloshing force on the TLD tank for the sinusoidal excitation applied on the tank walls [8] was predicted by the current numerical work. The time history of the normalized total sloshing force $\frac{F_{TLD}}{m_w\, g}$ was presented for excitation amplitude, A = 25.9mm, excitation frequency, $f = 0.594\, Hz$, and the phase shift angle, $\varphi = 4^0$, figure (5). Moreover the normalized sloshing force w.r.t. the excitation force was explained, figure (6). The direct examination of the time history of the normalized sloshing force, $\frac{F_{TLD}}{F_0 \sin(2\pi f t)}$ clear the non-uniform behavior of sloshing motion as the damping force was dominant in the time window of {15 seconds}starting after (4)seconds from the onset of excitation. On the other hand the serious events of sloshing motion reside when the total sloshing force and the excitation force coexisted.

Prediction of Wave Breaking

The formation of wave breaking near the wall side of TLD tank wall contains a liquid with shallow depth will be analyzed. The hydraulic jump was characterized by formation of nonlinear motion of the free surface followed by impact at the side wall and finally wave runner up and splashing occurs [38,39]. The current numerical investigate the free surface for TLD tank under excitation of amplitude {A=0.05m}, and of frequency of $f = 1.14\, Hz$, where the sloshing motion impacts the side wall and then hits the tank top [38]. The water depth inside TLD was $\{\frac{h}{L} = 0.35\}$, a value little differ from the critical depth needed to initiate a wave breaking, which assigned by Faltinsen [40], $\{\frac{h}{L} = 0.337\}$. The numerical prediction of free surface was illustrated on figure (7), where the numerical prediction of free surface superimposed on the snapshot of the excited free surface [39]. Figure (7) was represented for TLD subjected to sinusoidal excitation of amplitude {A=0.05m}, a frequency of 1.14 Hz, and at a time instant of {t = 19.4 T}, where [T] is the excitation period, and the ratio between the oscillation period [T] and the linear sloshing natural period [T_1] as$\{\frac{T}{T_1} = 1.107\}$. Moreover the current numerical work, figure (7) exhibit a good compatibility clears the verification of the use of the current numerical model to detect the free surface evolution of the sloshing liquid inside TLD in case of the hydraulic jump and wave breaking.

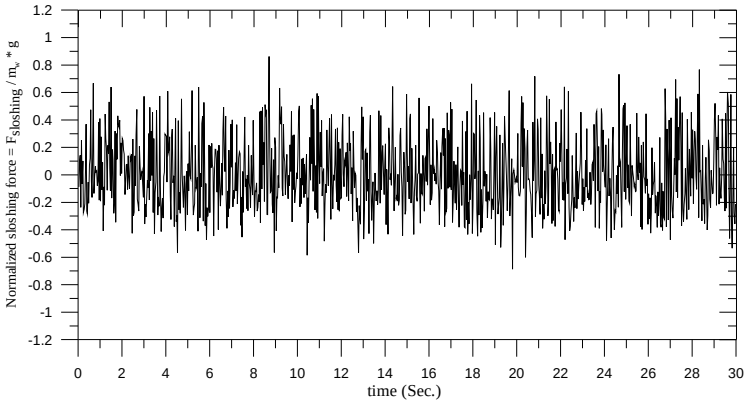

Figure 5 Time History of the Normalized Total Fluid Sloshing Force By the fluid weight, as Normalized force= $\frac{F_{TLD}}{m_w\, g}$, for excitation with sinusoidal wave of amplitude, A=0.259 cm with frequency of 0.59 Hz, and phase shift angle = 4^0 , [8].

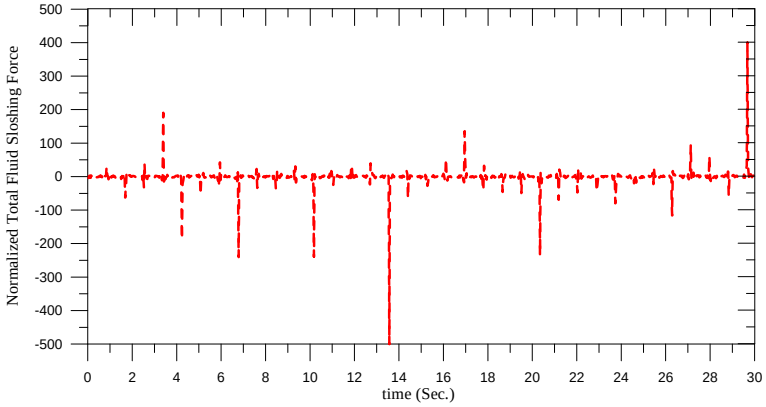

Figure 6 Time History of the Normalized Total Fluid Sloshing Force by the Sinusoidal Excitation Force, defined as:

Normalized force= $\frac{F_{TLD}}{F_0 \sin(2\pi f t)}$, for excitation with sinusoidal wave of amplitude, A=0.259 cm, with a frequency of 0.59 Hz, [8].

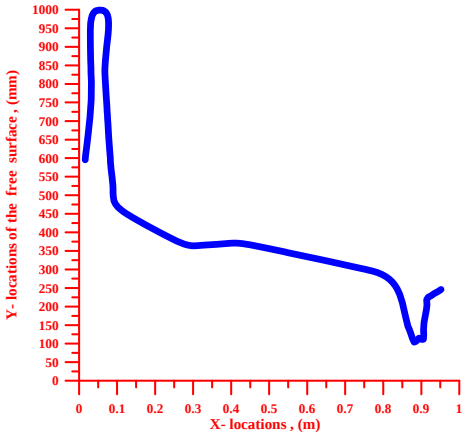

Figure 7(a)

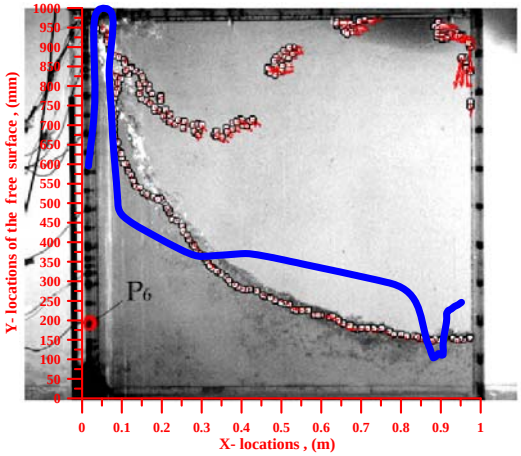

Figure 7(b)

Figure 7 The Numerical prediction of the free surface and the comparison with Snapshot at a time instant of t = 19.4 T of free surface, under the sinusoidal excitation with a frequency of 1.14 Hz and with amplitude, A= 0.05 m.

a) The current numerical prediction of free surface.

b) The numerical prediction of free surface superimposed on the snapshot of free surface and a direct comparison with SPH particles {white circles}, according to the work of A. Colagrossi [39].

SUMMARY AND CONCLUSIONS

The use of TLD in damping of the light scale vibration in due to wind excitation and the large scale excitation of the offshore platforms exhibits an effective dynamic absorber outweighs the other passive damping devices. A numerical model has been developed to predict the two-dimensional sloshing motion inside TLDs with an external sinusoidal excitation having different excitation frequencies. The current numerical model handles the free surface evolution by using the VOF method and the CSF model to handle the volume fluid force caused by surface tension.

The current numerical model proposes a new model for calculating pressure at the tank side walls. The onset of hydraulic jumps and wave breaking has been predicted. The current numerical model has been validated by direct comparison with experimental date reported in [8]. The predicted evolution of the free surface inside the TLD is in good agreement with the experimental data as compared to the experimental findings for the accurate detection of hydraulic jump [39].

ACKNOWLEDGMENT

The authors would like to acknowledge financial support of this research received from the Qatar National Research Fund through grant number NPRP 09 - 769 - 2 – 292.

REFERENCES

[1] M. Marivani, M.S. Hamed, Numerical investigation of Sloshing Motion inside Tuned Liquid Dampers with and without submerged screens", *PhD Thesis, McMaster University*, 2009.

[2] M. Marivani and M.S. Hamed, "Numerical Modeling of Sloshing Motion in a Tuned Liquid Damper Outfitted with a submerged Slat Screen", *Int. Journal of Numerical*

Methods in Fluids, available on-line January 12, 2010, 22 pages.

[3] K. Fujii , Y. Tamura, T. Sato, T. Wakahara, Wind-induced vibration of tower and practical applications of tuned liquid damper, *Journal of Wind Engineering and Industrial Aerodynamics*, Vol. 33,1990, pp. 263-72

[4] Kareem A. and Sun W.J. , Stochastic response of structures with fluid containing appendages, *Journal of Sound and Vibration* ,Vol. 21, 1987, pp. 389-408

[5] Matsuuara Y. , Matsumoto K. , Mizuuki M., Arima K. , Jouuchi H. , Hayashi S. ,On a mean to reduce excited vibration with the sloshing in a tank , *J. Soc. Naval. Architecture Japan*, Vol. 160, 1986, pp. 424-32

[6] Fujino Y. , Pacheco B.M. , Chaiseri P. , Fuji K., An experimental study on tuned liquid damper using circular containers, *JSCE Journal of Structural Engineering* ,Vol. 34 A, 1988, pp. 603-616

[7] Tamura Y. ,Fuji K. , Obtsuki P. , Pacheco B.M. , Effectiveness of tuned liquid dampers under wind excitations, *Engineering Structures*, Vol. 17,No.9 ,1995,pp. 609-621

[8] J. Hamelin, The effect of screen geometry on the performance of a Tuned Liquid Damper, *MSc. Thesis, McMaster University*, 2007.

[9] M.J. Tait, The performance of 1-D and 2-D Tuned Liquid Dampers, *Ph.D. Thesis, University of Western Ontario, London, Canada*, 2004.

[10] Abramson, H.N., The dynamic behavior of liquids in moving containers, *NASA SP-106, National Aeronautics and Space Administration. Washington, DC*, 1966.

[11] Armenio, V., Rocca, M.L., On the analysis of sloshing of water in rectangular containers: numerical study and experimental validation, *Ocean Engineering*, Vol. 23, No. 8, 1996, pp. 705–739

[12] Den Hartog J.P., Mechanical Vibrations, McGraw Hill, New York, 1956.

[13] Ruhl J.A., Offshore platforms: observed behavior and comparisons with theory, *J. Petrol. Technol.*, Vol. 30, 1978.

[14] Nakayama T. and Washizu K. The boundary element method applied to the analysis of two dimensional nonlinear sloshing problems, *International Journal of Numerical Methods In Engineering*, Vol. 17, 1981, pp. 1631-46

[15] Reed D. , Jinkyu Y., Harry Y., Investigation of tune liquid dampers under large amplitude excitation, *Journal of Engineering Mechanics, ASCE*, Vol. 124, No. 4, 1998.

[16] Y. Zang, S. Xue, S. Kurita, A boundary element method and spectral analysis model for small-amplitude viscous fluid sloshing in couple with structural vibrations, *International Journal for Numerical Methods in Fluids*, Vol. 32, 2000, pp. 79-96

[17] T.G. Lepelletier , and F. Raichlen , Nonlinear oscillations in rectangular tanks, *Journal of Engineering Mechanics* ,Vol. 114, 1988, pp. 1-23

[18] Y. Kim, Numerical simulation of sloshing flows with impact load, *Appl. Ocean Res.*, Vol. 23, 2001, pp. 53–62

[19] Y. Kim, Y.-S. Shin, K.H. Lee, Numerical study on slosh-induced impact pressures on 3-D prismatic tanks, *Appl. Ocean Res.* ,Vol. 26, 2004, pp. 213-226

[20] Dongming Liu , Pengzhi Lin , A numerical study of three-dimensional liquid sloshing in tanks, *Journal of Computational Physics*, Vol. 227, 2008, pp. 3921-39

[21] Lax. P. D., and Wendroff. B., Difference schemes for hyperbolic equations with high order of accuracy. *Communications on Pure and Appl. Math.*, Vol. 17, 1964, pp. 381-398

[22] Glimm. J., Solution in the large for nonlinear hyperbolic systems of equations, *Communications on Pure and Appl. Math.*, Vol. 18, 1965, pp. 697-715

[23] Holt, M., Numerical methods in fluid dynamics, Springer-Verlag KG. Berlin. Germany, 1984.

[24] Gardarsson. S., and Yeh. H., Numerical simulations of bores using the random-choice method, *Proc., 3rd UJNR Tsunami Workshop, Public Works Research Council, Ministry of Construction, Tsukuba, Japan*, 1994, pp. 13-23

[25] Reed D., Yu J., Yeh. H., and Gardarsson. S., Investigation of Tuned Liquid Dampers under Large Amplitude Excitation, *J. of Engr. Mech.*, April 1998.

[26] Nichols B. D., Hirt C. W., *Proceedings First Intern. Conf. Num. Ship Hydrodynamics, Gaithersburg, Md*, October 1975.

[27] McMaster W.H., and Gong E. Y., PELE-1C User's Manual, *Lawrence Livermore Laboratory report UCRL-52609*, 1979.

[28] Hirt C. W., Nichols B. D., Volume of Fluid Method (VOF) Method for the Dynamics of Free Boundaries, *J. Comp. Phys.* , Vol. 39 ,1981, pp. 201-225

[29] J. U. Brackbill, D. B. Kothe, And C. Zemach,"A Continuum Method For Modeling Surface Tension", *Journal Of Computational Physics*, Vol. 100, 1992, pp. 335-354

[30] Patankar S. V., and Spalding D.B., Mathematical Models Of Turbulence ,Academic Press Inc. (London) , Fifth Edition, 1972.

[31] P.K. Panigrahy, U.K. Saha , D. Maity , Experimental studies on sloshing behavior due to horizontal movement of liquids in baffled tanks, Ocean Engineering ,Vol. 36 ,2009, pp. 213–222

[32] Dongming Liu, Pengzhi Lin, Three-Dimensional liquid sloshing in a tank with baffles, *Ocean Engineering*, Vol. 36, 2009, pp. 202-212

[33] Dietmar Rempfer, On Boundary Conditions for Incompressible Navier – Stokes Problems, *Applied Mechanics Review, Transactions of ASME*, Vol. 59, May 2006, pp. 107-125

[34] Frank M. White, Fluid Mechanics, McGraw Hill, 1979.

[35] P. Pal, and S.K. Bhattacharyya, Sloshing In Partially Filled Liquid Containers-Numerical and Experimental Study for 2-D Problem, *Journal of Sound and Vibration*, Vol. 329, 2010, pp. 4466-4485

[36] Colagrossi, A., C. Lugni, M. Greco, and O. Faltinsen, Experimental And Numerical Investigation Of 2D Sloshing : Scenarios Near The Critical Filling Depth, *In*

Proc. 19th International Workshop on Water Waves and Floating Body, Cortona, Italy, 2004.

[37] Oda T. F., Hamed M.S., Saud Ghani , Numerical modeling of Wave Breaking Inside Tuned Liquid Dampers submitted to *International JournalfFor Numerical Methods In Fluids*, 2012.

[38] Y. Kim, experimental and numerical analyses of sloshing flows, *J. Eng. Math.*, Vol. 58, 2007, pp. 191-210

[39] Colagrossi, A., C. Lugni, M. Greco, and O. Faltinsen, Experimental And Numerical Investigation Of 2D Sloshing with Slamming, *In Proc. 19th International Workshop on Water Waves and Floating Body, Cortona, Italy*, 2004.

[40] Faltinsen O., O. R. I. Lukovskyand, and A. Timokha, Multidimensional modal analysis of nonlinear sloshing in a rectangular tank with finite water depth, *J. Fluid Mech.*, Vol. 407, 2000, pp. 201–234

[41] R.A. Ibrahim, Liquid Sloshing Dynamics: Theory and Applications, Cambridge University Press, New York, USA, 2005.